Polymer Chemistry

ROYAL SOCIETY OF CHEMISTRY

PAPER

View Article Online
View Journal | View Issue

Cite this: *Polym. Chem.*, 2022, **13**, 5568

pH-Responsive, two-in-one doxorubicin and Bcl-2 siRNA-loaded micelleplexes for triple-negative breast cancer therapy†

Hung-Hsun Lu,‡[a,c] Hsueh Wen Liu,‡[a,c] Trinh Kieu Dinh,[b,c] Cheng-Hung Huang,[a,c] Hsi-Chien Huang,[b,c] Ya-Ching Tseng,[a,c] Man-Hsuan Ku,[a,c] Fu-Sheng Wang,[a,c] Yunching Chen *[b,c] and Chi-How Peng *[a,c]

The combination of chemotherapy and gene therapy is a versatile strategy for treating multi-drug-resistant cancer. Accordingly, we developed a pH-responsive triblock copolymeric carrier for delivering chemotherapeutic and genetic drugs simultaneously. We synthesized a series of block and random copolymers with the same monomer composition, namely poly(ethylene glycol)-*b*-poly(2-(dimethylamino)ethyl methacrylate)-*b*-poly(2-(diisopropylamino)ethyl methacrylate) (PEG-*b*-PDMAEMA-*b*-PDPA) and poly(ethylene glycol)-*b*-poly[(2-(dimethylamino)ethyl methacrylate)-*r*-(2-(diisopropylamino)ethyl methacrylate)] (PEG-*b*-(PDMAEMA-*r*-PDPA)), by using atom transfer radical polymerization (ATRP) and then used them to encapsulate and release doxorubicin (Dox) and Bcl-2 siRNA. Compared with the random copolymers, the block copolymers exhibited a higher Dox-loading efficiency and Dox-loading capacity and higher Bcl-2 siRNA condensation efficiency. The siRNA condensation efficiency could be increased by increasing the length of the PDMAEMA segment in either the block copolymers or random copolymers. PEG-*b*-PDMAEMA-*b*-PDPA encapsulated Dox and Bcl-2 siRNA to form Dox/Bcl-2 siRNA-loaded micelleplexes with 87% and 90% loading efficiency, respectively. Changing the pH value from 7.4 to 5.0 engendered a burst release of Dox and Bcl-2 siRNA from the Dox/Bcl-2 siRNA-loaded micelleplexes, thus enhancing the cumulative release efficiency of Dox from 24% to 69% and that of Bcl-2 siRNA from 15% to 59% within 24 h. Our *in vitro* study revealed that the Dox/Bcl-2 siRNA-loaded micelleplexes downregulated Bcl-2 mRNA expression (51% expression) and further inhibited antiapoptotic mechanisms to sensitize drug-resistant triple-negative breast cancer (TNBC) cells to Dox (36% cell viability); this thus demonstrates the benefits of combining chemotherapy and gene therapy.

Received 23rd February 2022,
Accepted 30th August 2022

DOI: 10.1039/d2py00246a

rsc.li/polymers

Introduction

Chemotherapy has been a universal cancer treatment in clinical practice for several decades. However, chemotherapy still involves several challenges, particularly the high rate of cancer recurrence and low drug response after consecutive treatments due to cancer heterogeneity and acquired resistance.[1–4] Triple-negative breast cancer (TNBC), which occurs in 10%–20% of patients with breast cancer,[5,6] is associated with a substantially low survival rate. The standard-of-care treatment for TNBC is limited to chemotherapy because TNBC tumors are characterized by the lack of expression of estrogen receptor (ER), progesterone receptor (PR), and human epidermal growth factor receptor 2 (HER2).[6,7] Patients with TNBC usually encounter a gradual decline in drug response after multiple chemotherapy sessions, which can be attributed to the overexpression of survival genes associated with antiapoptotic pathways or drug efflux pumps.[8,9] Gene therapy using small-interfering RNA (siRNA), which silences the targeted mRNA through the cleavage of the RNA-induced silencing complex (RISC) machinery in cancer cells, shows promise as a modality of deactivating drug resistance pathways.[10–12] Combining gene therapy with conventional chemotherapy can substantially enhance the drug response in the treatment of multi-drug-resistant cancer.[13–18]

[a]*Department of Chemistry, National Tsing Hua University, 101, Sec 2, Kuang-Fu Rd., Hsinchu 30013, Taiwan. E-mail: chpeng@mx.nthu.edu.tw*
[b]*Institute of Biomedical Engineering, National Tsing Hua University, 101, Sec 2, Kuang-Fu Rd., Hsinchu 30013, Taiwan. E-mail: yunching@mx.nthu.edu.tw*
[c]*Frontier Research Center on Fundamental and Applied Sciences of Matters, National Tsing Hua University, 101, Sec 2, Kuang-Fu Rd., Hsinchu 30013, Taiwan*

†Electronic supplementary information (ESI) available: The materials and instruments, details of the synthesis and characterization of polymers, formulation of the micelles and micelleplexes, siRNA and Dox release profiles, measurements of cell viability and cellular uptake are provided in the supporting information. See DOI: https://doi.org/10.1039/d2py00246a

‡These authors equally contributed to this work.

Although siRNA performs efficiently within RNA interference pathways, it is vulnerable to serum and endonuclease in physiological environments.[11,19–22] Over the past few decades, considerable advances have been made in the study of polycations, which can spontaneously stabilize negatively charged siRNA to form polyplexes or micelleplexes and prevent siRNA degradation.[23–26] Reineke *et al.* tested a wide variety of glycopolycations, comprising glucose and amine-containing monomers with various degrees of methyl substitution, and reported that the polymer structure (statistical and block) and chain length influenced gene binding affinity, colloidal properties, material cytotoxicity, cellular internalization, and transfection efficiency for gene and protein therapy.[27–37] Duvall *et al.* demonstrated that the balance of hydrophobic and cationic segments of pH-responsive siRNA polyplexes could enhance endosomal escape, stability, blood circulation half-life, and bioactivity *in vivo*.[38] Furthermore, a study used a series of siRNA polyplexes composed of various polymers and thus having different N/P ratios (number of amines on the polymer/number of phosphates on the siRNA) to demonstrate the influence of the composition, complex formulation, and surface density of poly(ethylene glycol) on its particle size, surface charge, colloidal stability, and bioactivity *in vivo*.[39] Accordingly, polymer structure and composition play a vital role in drug formulation and gene delivery *in vitro* and *in vivo*.

On the basis of the findings of research on the combination of chemotherapy and gene therapy and those of research on the influence of polymer composition and structure on drug delivery, we designed a pH-responsive triblock copolymer that can simultaneously encapsulate doxorubicin (Dox) and Bcl-2 siRNA to achieve both chemotherapy and gene therapy. We also studied the effects of monomer sequence and cationic segment chain length on siRNA condensation and release profiles. A series of copolymers, namely poly(ethylene glycol)-*b*-poly(2-(dimethylamino)ethyl methacrylate)-*b*-poly(2-(diisopropylamino)ethyl methacrylate) (PEG-*b*-PDMAEMA-*b*-PDPA) and poly(ethylene glycol)-*b*-poly[(2-(dimethylamino)ethyl methacrylate)-*r*-(2-(diisopropylamino)ethyl methacrylate)] (PEG-*b*-(PDMAEMA-*r*-PDPA)) with different DMAEMA chain lengths (Scheme 1A), were synthesized using atom transfer radical

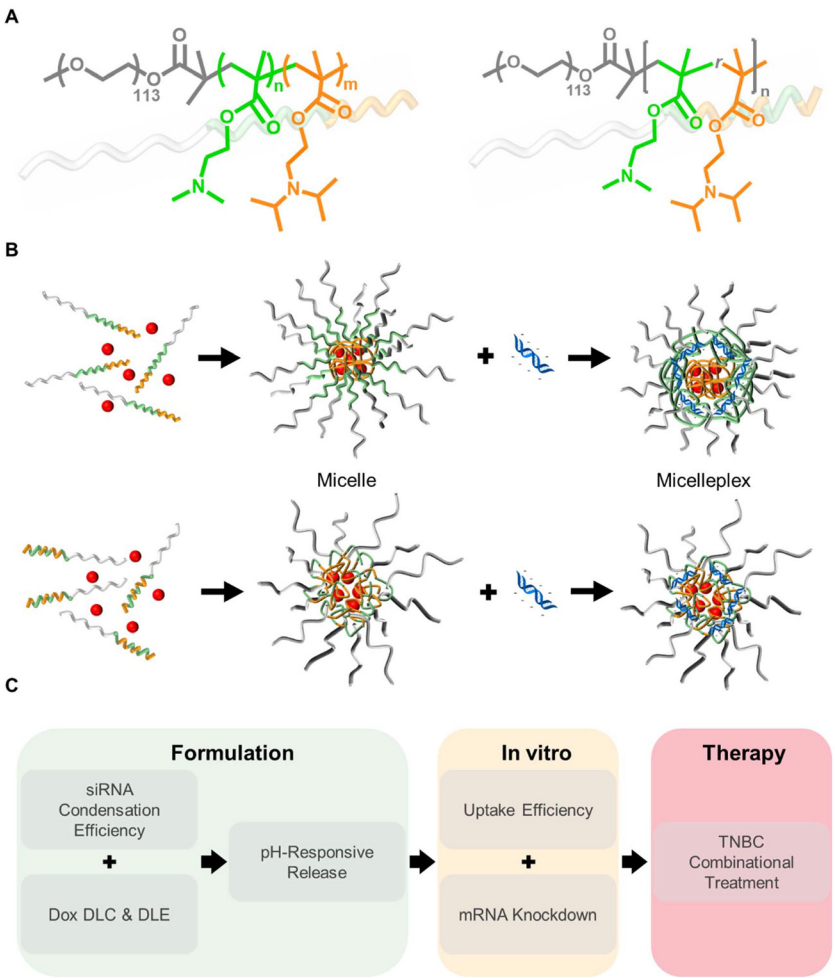

Scheme 1 Schematic of (A) chemical structure of PEG-*b*-PDMAEMA-*b*-PDPA and PEG-*b*-(PDMAEMA-*r*-PDPA) copolymers; (B) sequential formation of self-assembled copolymers, Dox-loaded micelles, and Dox/Bcl-2 siRNA-loaded micelleplexes; and (C) selection strategy for copolymer candidates for the efficacious formulation of a combination drug delivery system.

polymerization (ATRP).[40] PEG was used as the outer layer of the micelleplex, providing biocompatibility and preventing aggregation. PDMAEMA could carry a positive charge at an appropriate pH value to condense the negatively charged siRNA through electrostatic interactions. PDPA could serve as the hydrophobic core of the micelleplex and could stabilize Dox in the core (Scheme 1B). We first evaluated the siRNA condensation efficiency as well as the Dox drug-loading efficiency (DLE) and drug-loading capacity (DLC) by using the synthesized copolymers as the carrier (Scheme 1C). The Dox/Bcl-2 siRNA-loaded micelleplexes with PEG_{113}-*b*-$PDMAEMA_{55}$-*b*-$PDPA_{59}$ exhibited loading efficiency levels of approximately 87% and 90%, respectively. The pH value was switched from 7.4 to 5.0, triggering a pH-responsive release, as evidenced by the increase in cumulative release from 24% to 69% for Dox and 15% to 59% for Bcl-2 siRNA in 24 h. In the *in vitro* study, the uptake efficiency of the micelleplexes was higher than that of free siRNA by fivefold, and the expression of Bcl-2 mRNA in MDA-MB-231 cells was suppressed by more than 50% compared with that in control cells. In particular, the copolymer delivery system comprising the Dox/Bcl-2 siRNA-loaded micelleplexes exhibited superior therapeutic efficacy compared with single delivery systems comprising Dox-loaded micelles and Bcl-2 siRNA-loaded micelleplexes; this thus indicates that this triblock copolymeric delivery system could be a two-in-one platform for combination therapy for TNBC.

Results and discussion

Polymer synthesis and self-assembled structure

We synthesized a series of block and random copolymers, namely PEG-*b*-PDMAEMA-*b*-PDPA and PEG-*b*-(PDMAEMA-*r*-PDPA), by using ATRP, with CuBr/PMDETA serving as the catalyst, PEG_{113}-Br (M_n = 5000 g mol^{-1}, $Đ$ = 1.03) serving as the initiator, and Cu(0) serving as the reducing agent in anisole at 40 °C. Sequential chain extension reactions were conducted on PDMAEMA and PDPA (Scheme S1A†) to yield triblock copolymers that exhibited varying degrees of polymerization (DPs) of the PDMAEMA segment (DP = 18, 41, and 55), similar PDPA chain lengths (DP = 54–59), molecular weights of 19 100, 22 600, and 25 500, and polydispersity ($Đ$) values of approximately 1.17–1.27. Random copolymers were prepared through the copolymerization of DMAEMA and DPA (Scheme S1B†) to yield a molecular weight and composition similar to that of the corresponding block copolymers. Table 1 presents the characteristics of three triblock copolymers and three random copolymers derived from PEG-*b*-(PDMAEMA-*r*-PDPA) (denoted as LR, MR, and SR, corresponding to long, medium, and short PDMAEMA chain lengths, respectively) and PEG-*b*-PDMAEMA-*b*-PDPA (denoted as LB, MB, and SB, corresponding to long, medium, and short PDMAEMA chain lengths, respectively). The repeating unit and number-average molecular weight ($M_{n,\ NMR}$) of PDMAEMA and PDPA were calculated using ^{1}H nuclear magnetic resonance (NMR) spectra, and the molecular weight distribution was determined through gel permeation chromatography (GPC).

Table 1 Characteristics of PEG-*b*-(PDMAEMA-*r*-PDPA) and PEG-*b*-PDMAEMA-*b*-PDPA

Entry	$M_{n,\ NMR}$[a] (g mol^{-1})	$Đ$[b]	DP[c] DMAEMA	DP[c] DPA	D_n[d] (nm)	PDI[d]
PEG-*b*-(PDMAEMA-*r*-PDPA)						
SR	20 200	1.16	20	58	23.37	0.247
MR	22 300	1.22	36	57	31.47	0.177
LR	25 000	1.18	58	55	32.53	0.219
PEG-*b*-PDMAEMA-*b*-PDPA						
SB	19 100	1.17	18	54	25.70	0.208
MB	22 600	1.27	41	55	23.50	0.235
LB	25 500	1.25	55	59	22.97	0.245

[a] Molecular weight determined by ^{1}H NMR. [b] Polydispersity measured by GPC using THF/LiBr as eluent. $Đ = M_w/M_n$. [c] Degree of polymerization calculated by ^{1}H NMR. [d] *Z*-Average size of nanoparticles and distribution in DIW determined by DLS.

Dynamic light scattering (DLS) analysis revealed that these block and random copolymers could self-assemble into nanoparticles through nanoprecipitation under ultrasonication[41] This finding was validated by the hydrophobicity of PDPA that constituted the core of the micelle and by the hydrophilicity of PEG and PDMAEMA that remained on the sphere and prevented micelle aggregation. Micelles derived from these polymers exhibited a relatively consistent particle size that ranged between 23 and 33 nm and had a particle size distribution (PDI) of approximately 0.22 (Table 1). However, the correlation between particle size and molecular weight was nonsignificant; this could be attributed to the loose micelle structure, meaning that the particle size was not sensitive to the difference in chain length among the polymers. We subsequently used these polymers to investigate the influence of monomer sequence on the formulation of the two-in-one delivery system.

Structure-dependent formulation of block and random copolymers with siRNA

Both PEG-*b*-PDMAEMA-*b*-PDPA and PEG-*b*-(PDMAEMA-*r*-PDPA) were expected to form micelleplexes loaded with siRNA and to condense the loaded siRNA in the polycationic layer through an electrostatic interaction between positively charged amines on DMAEMA and negatively charged phosphates on siRNA (Scheme S2†). The micelleplexes were formed by mixing an siRNA stock solution at a constant volume and a micelle solution at various N/P ratios simultaneously. The N/P ratio was used to quantify the condensation efficiency of the gene carrier. We used agarose gel electrophoresis along with ethidium bromide staining to assess the siRNA condensation efficiency of the synthesized block and random copolymers (Fig. 1). Various polymer concentrations were added to the siRNA stock solution in a phosphate-buffered environment (pH 7.4; ionic strength = 10 mM) to encapsulate siRNA with the desired N/P ratios (N/P = 1, 5, 10, 15, 20). The qualitative assessment results revealed that the LB and MB copolymers exhibited the highest siRNA condensation efficiency, which increased with the N/P ratio. Although the LR copolymer

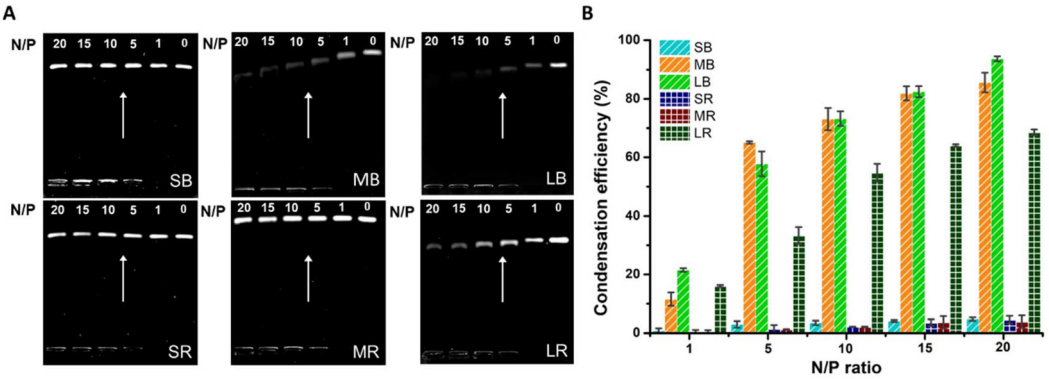

Fig. 1 (A) Gel electrophoresis of siRNA-condensed SB, MB, LB, SR, MR and LR micelleplexes. The arrow indicates where the siRNA shift occurred. (B) siRNA condensation efficiency of SB, MB, LB, SR, MR and LR micelleplexes at various N/P ratios determined by the quantification of ethidium bromide fluorescence in the siRNA band using ImageJ analysis software.

exhibited a relatively high siRNA condensation efficiency level, the SB, SR, and MR did not show adequate siRNA condensation efficiency, even when the N/P ratio was as high as 20 (Fig. 1A). The LB and MB copolymers had similar condensation efficiency levels, which exceeded 70% at an N/P ratio of 10 and approached 90% at an N/P ratio of 20. However, the SB copolymer had a condensation efficiency of only 5%, even when the N/P ratio was 20; this finding is consistent with that reported by a previous study that a longer cationic PDMAEMA chain is associated with a higher siRNA condensation efficiency.[42] Accordingly, we selected the micelleplex composed of LB and siRNA for our subsequent stability test, which demonstrated that the micelleplex exhibited consistent condensation efficiency levels when preserved at 4 °C for a week (Fig. S1†). Moreover, the results revealed that the random SR and MR copolymers could barely carry the loaded siRNA (<5% efficiency at an N/P ratio of 20). Despite the LR copolymer achieving a condensation efficiency level of 70% at an N/P ratio of 20, the random copolymers had lower siRNA condensation efficiency levels than did the corresponding block copolymers (Fig. 1B). This finding implies that the random sequence of DMAEMA and DPA prevented the PDMAEMA segment from binding with the siRNA. On the basis of the preceding results, we can determine that even with the same polymer composition, the macromolecular design, such as the sequence of monomers and the chain length of the cationic segment, has a substantial effect on the self-assembled structure and formulation of siRNA carriers.

Structure-dependent formulation of block and random copolymers with Dox and siRNA

We designed the PDPA segments in PEG-*b*-PDMAEMA-*b*-PDPA and PEG-*b*-(PDMAEMA-*r*-PDPA) to incorporate Dox into their cores by leveraging their hydrophobicity, thus enabling payload delivery through a hydrophobic-to-hydrophilic transition in an acidic environment. We loaded Dox into the micelles through the nanoprecipitation of the Dox and copolymer solution under sonication (Scheme S3†); subsequently, we derived the DLE and DLC of the copolymers through the precipitation of Dox in a dialysis bag against a phosphate-buffered solution (pH 7.4, 20 mM). All three block copolymers could capture Dox, with their DLE and DLC exceeding 75% and 10%, respectively. However, the DLE and DLC of the PEG-*b*-(PDMAEMA-*r*-PDPA) copolymers were 41%–49% and 7.2%–8.4% (Table 2), respectively, which were lower than those of the block copolymers; this finding indicates that the random distribution of the DPA monomers weakened the hydrophobicity of the copolymers, reducing the amount of Dox that could be stabilized in the core. We executed DLS to determine changes in micelle size before and after Dox loading. The results showed that for the block copolymers, the micelle size increased after Dox loading; the explanation for this finding is that the block copolymers had a more regulated structure in which PDMAEMA-*b*-PEG surrounded the PDPA block in the core to ensure that the encapsulated Dox enlarged only the core, leading to an increase in particle size after Dox loading. For the random copolymers, the micelle size decreased after Dox loading; the explanation for this finding is that PDMAEMA-*r*-PDPA loosely constituted the micelle core, and the addition of Dox enhanced the hydrophobic interaction in the core and dragged the DPA monomers to form a denser

Table 2 Hydrodynamic diameter (D_h) of self-assembled copolymers and drug-loaded self-assembled copolymers, as determined using DLS, and corresponding DLE[a] and DLC[b] values

Entry	DLE[a] (%)	DLC[b] (%)	Size (nm) without DOX	Size (nm) with DOX
SR	41.6	7.2	25.4 ± 0.9	31.8 ± 2.7
MR	44.5	7.7	32.8 ± 2.1	23.4 ± 1.9
LR	48.7	8.4	33.5 ± 0.4	16.2 ± 1.9
SB	75.0	10.1	28.7 ± 1.3	34.2 ± 4.1
MB	77.1	10.4	27.5 ± 0.8	28.1 ± 3.8
LB	86.9	11.4	28.9 ± 0.7	34.2 ± 2.4

[a] DLE (%) = (weight of loaded Dox/weight of Dox in feed) × 100. [b] DLC (%) = [weight of loaded Dox/(weight of Dox + polymers)] × 100.

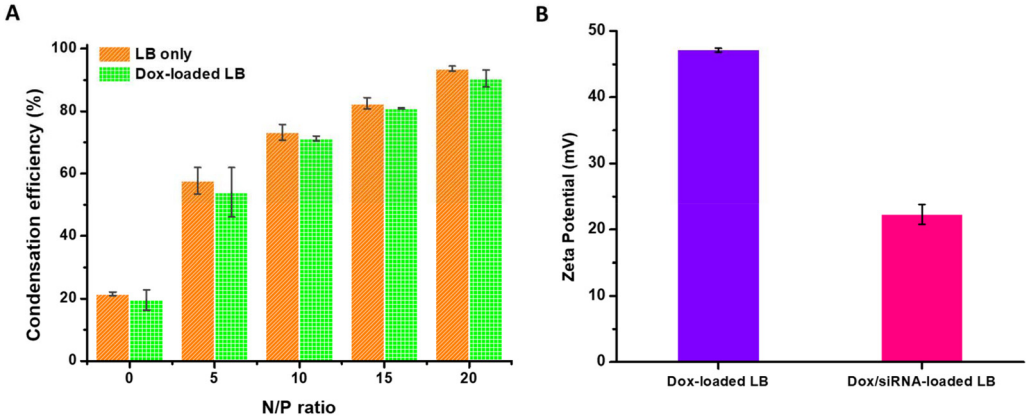

Fig. 2 (A) Comparison of siRNA condensation efficiency between LB micelles and Dox-loaded LB micelles. (B) Zeta potential of Dox-loaded LB micelles before and after siRNA condensation.

core, thus resulting in a decrease in particle size. The encapsulation of Dox was further confirmed by the quenched fluorescence of Dox (Fig. S2†), which was attributed to the π–π stacking interaction between Dox molecules in the constrained core. Consider, for example, the LB copolymers: the Dox-loaded LB micelles exhibited high stability when preserved at 4 °C for a week, and this was supported by the release profile of the Dox-loaded LB micelles in the dialysis bag against the phosphate-buffered solution (pH 7.4, 140 mM); this profile demonstrated a cumulative release of less than 10% in a week (Fig. S3†). Furthermore, we assessed the particle size of the Dox-loaded LB micelles over a 1-week period by using DLS analysis, which revealed a consistent hydrodynamic diameter (D_h) and count rate throughout the assessment period (Fig. S4†).

Because the Dox-loaded LB micelles exhibited prominent DLE and DLC results, they were selected for further analysis of siRNA condensation. The Dox-loaded LB micelles were added to an siRNA stock solution at predetermined N/P ratios to prepare Dox/Bcl-2 siRNA-loaded micelleplexes. The Dox-loaded micelles exhibited similar siRNA condensation efficiency levels with the empty LB micelles at various N/P ratios (Fig. 2A), signifying that the encapsulation of Dox within the hydrophobic core had no considerable effect on the siRNA condensation efficiency of the cationic PDMAEMA block. Furthermore, our DLS analysis results revealed that the zeta potential of the Dox-loaded micelleplexes dropped from 47 to 22 mV after siRNA condensation, suggesting that siRNA was condensed in the PDMAEMA layer of the Dox-loaded LB micelles through an electrostatic interaction (Fig. 2B).

pH-Responsive release profiles of siRNA and Dox

Studies developing ultra-pH-sensitive fluorescence probes composed of fluorogen-conjugated poly(ethylene glycol)-*b*-poly(2-(diisopropylamino)ethyl methacrylate) have reported that the hydrophobic-to-hydrophilic transition of protonable PDPA is a pH trigger in these probes.[43–46] Accordingly, we expected that the PDPA block could respond to changes in pH and lead to supramolecular disassembly; we thus evaluated the range of pH and the sensitivity corresponding to the hydrophobic-to-hydrophilic transition of PDPA (Fig. 3A). The pH-dependent DLS analysis results demonstrated that the LB micelles were stable in the basic environment; they exhibited a particle size of 28 nm and light-scattering intensity of 274 kcps. Their particle size and light-scattering intensity began to decrease when the pH value was lower than 7.4, and they dropped to 13 nm and 85 kcps, respectively, when the pH value was 6.8 (Fig. 3B and C). The pH interval ($\Delta pH_{10-90\%}$), which was defined as the pH range associated with a 10%–90% difference in pH change compared with the original data,[47] was calculated to be 0.24. The median of the pH interval, defined as the pH associated with the phase transition (pH_t), was determined to be 6.88. The dramatic changes in particle size and light-scattering intensity were attributed to the supramolecular disassembly induced by the protonation of the PDPA block. This explanation was supported by transmission electron microscopy (TEM) images, in which the micelles exhibited an intact structure at pH values of 7.4 and 7.0 but were barely identifiable at a pH value of 6.5 (Fig. 3D). Accordingly, PEG-*b*-PDMAEMA-*b*-PDPA formed micelles when the pH value exceeded 7.4. Lowering the pH value led to the protonation of the PDPA segment, which weakened the hydrophobic interactions in the core. Further increasing the acidity level could ensure the completion of the hydrophobic-to-hydrophilic transition of PDPA and thus disassemble the micelles to unimers. According to the narrow pH interval as well as the derived pH value for the phase transition, the LB micelles should be an ideal carrier for pH-responsive Dox/siRNA release.

To determine the pH-responsive release profiles for Dox and siRNA, we assessed the cumulative release efficiency of Dox and siRNA from the Dox/Bcl-2 siRNA-loaded LB micelleplexes (Fig. 4) in a phosphate-buffered solution (pH 7.4; 20 mM; ionic strength = 0.14 M) and acetate buffer (pH 5.0; 20 mM; ionic strength = 0.14 M). At a pH value of 7.4, the cumulative release efficiency of Dox from the micelleplexes was 24% after 24 h, and it steadily approached 40% after 96 h. By contrast, at a pH value of 5.0, the micelleplexes exhibited

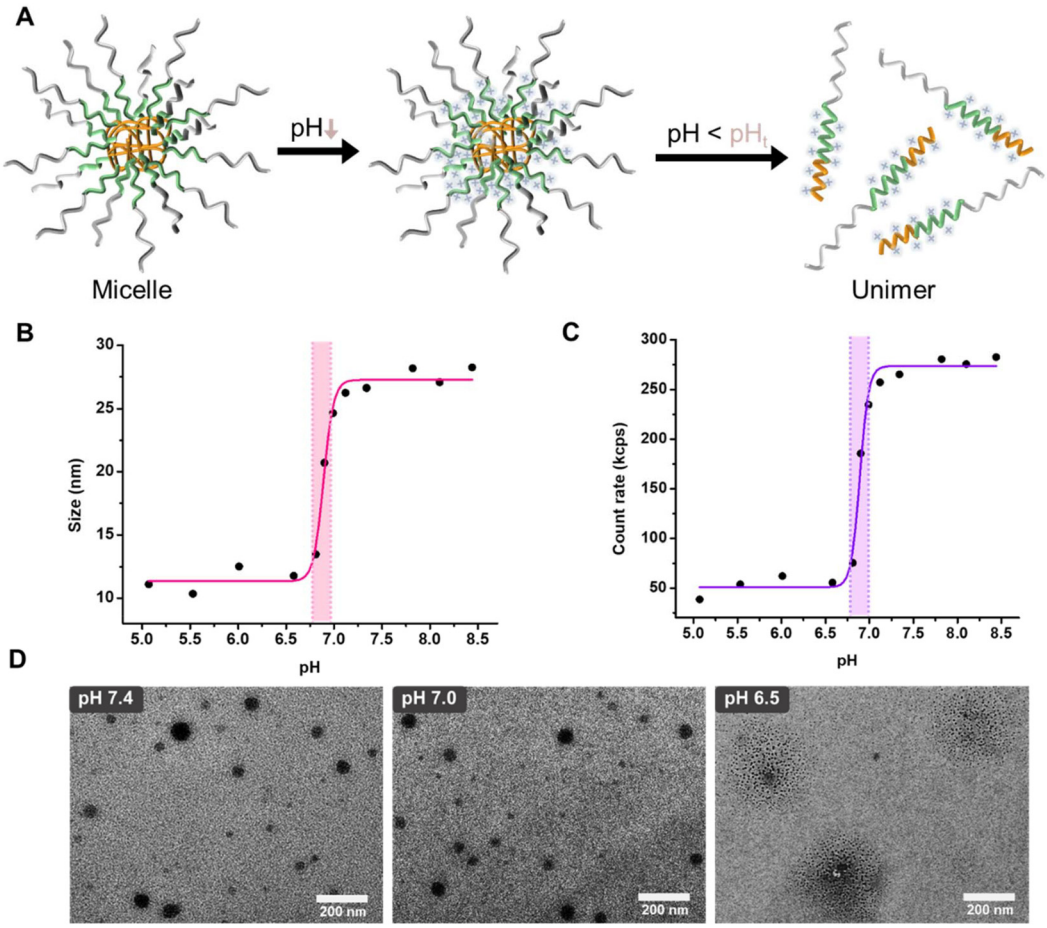

Fig. 3 pH-Responsive disintegration of self-assembled LB micelles. (A) Illustration of pH-responsive disintegration of LB micelles in a cascade. Changes in (B) hydrodynamic diameter and (C) scattering intensity (count rate) of self-assembled LB micelles (0.1 mg mL^{-1}) with HCl (0.1 M) titration. (D) Representative TEM images of self-assembled LB micelles (0.5 mg mL^{-1}) at pH 7.4, 7.0, and 6.5 cast on a carbon/Formvar-coated copper TEM grid and negatively labeled with 1% phosphotungstic acid (PTA). Scale bar: 200 nm.

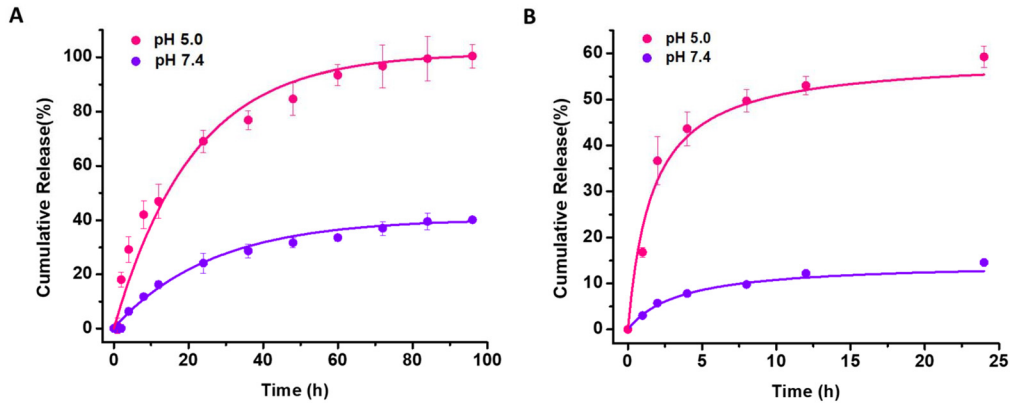

Fig. 4 Cumulative (A) Dox and (B) siRNA release profiles of Dox/Bcl-2 siRNA-loaded LB micelleplexes at 37 °C in phosphate-buffered solution (pH 7.4; 20 mM; ionic strength = 0.14 M) and acetate buffer (pH 5.0; 20 mM; ionic strength = 0.14 M).

burst release of Dox, with the cumulative release efficiency being 69% after 24 h; the cumulative release efficiency gradually reached >99% after 96 h, indicating the release of the entirety of the encapsulated Dox (Fig. 4A). Regarding siRNA release, we calculated the cumulative release efficiency by using a previously reported ultracentrifugation method to collect liberated FAM-labeled siRNA from the solution.[48] The results revealed that at a pH value of 5.0, the Dox/Bcl-2 siRNA-

loaded LB micelleplexes exhibited a cumulative release efficiency of 59.2% after 24 hours, considerably exceeding the value of 14.6% observed at a pH value of 7.4 (Fig. 4B). We validated the feasibility of the aforementioned ultracentrifugation method by conducting a control assessment involving free siRNA; the results indicated a release efficiency of approximately 90% within 1 h (Fig. S5†). The significant increase in release efficiency for both Dox and siRNA could be attributed to the pH-induced dissociation of the PDPA core in the micelleplexes. This thus suggests that the Dox/Bcl-2 siRNA-loaded LB micelleplexes could selectively release Dox and siRNA in the acidic late endosome/lysosome environment, preventing premature leakage and releasing the encapsulated payload on demand.

Material cytotoxicity

We tested the cytotoxicity of the LB micelles by conducting a 3-(4,5-dimethylthiazol-2-yl)-2,5-diphenyltetrazolium bromide (MTT) assay on MDA-MB-231 cancer cells. The LB micelle concentration was set to 1.5–15 μg mL^{-1} because 15 μg mL^{-1} of LB micelles could carry approximately 100 nM siRNA and 3.07 μM (1.67 μg mL^{-1}) Dox, which exceeded the dose used for *in vitro* research. The MDA-MB-231 cells were treated with the LB micelles for 6 h and then incubated for another 24 h; MDA-MB-231 cells without treatment were used as controls. We observed that the treatment with various concentrations of LB micelles did not lead to an effective decrease in the viability of the treated cells compared with the control cells (Fig. 5), signifying that a PEG-*b*-PDMAEMA-*b*-PDPA concentration of <15 μg mL^{-1} should not be harmful to cells.

In vitro cellular uptake

We applied confocal laser scanning microscopy (CLSM) to assess the intracellular delivery performance of the Dox/siRNA-loaded LB micelleplexes; for this assessment, the siRNA and Dox concentrations were set to 75 nM and 3 μg mL^{-1}, respectively. The derived CLSM images are depicted in Fig. 6A (original-size images are depicted in Fig. S18–S22†). Moreover, siRNA was labeled with FAM and visualized in green fluorescence, Dox was visualized in red fluorescence, and MDA-MB-231 cancer cell nuclei were labeled with DAPI and visualized in blue fluorescence. For the control cells with free Dox and free FAM-labeled siRNA, only a small amount of Dox was absorbed, and the cellular uptake efficiency of free FAM-labeled siRNA was extremely low. The Dox/siRNA-loaded LB micelleplexes were effective in delivering Dox and FAM-labeled siRNA into the nuclei, as confirmed by the enhanced fluorescence intensity and by the overlap of fluorescence with different colors. Furthermore, the Dox/siRNA-loaded LB micelleplexes could simultaneously deliver both Dox and FAM-labeled siRNA to the cytoplasm, as indicated by the overlap of all three fluorescence. We quantitatively analyzed the cellular uptake of Dox and FAM-labeled siRNA in the MDA-MB-231 cancer cells by calculating the average optical density (AOD) of Dox and FAM-labeled siRNA in the CLSM images. The uptake efficiency of free Dox and that of free siRNA were calibrated as 1 for comparison with the number of payloads delivered by the Dox-loaded micelles, Bcl-2 siRNA-condensed micelleplexes, and Dox/siRNA-loaded micelleplexes. The uptake efficiency levels of the Dox-loaded micelles and the Dox/siRNA-loaded micelleplexes were both higher than that of free Dox by approximately twofold (Fig. 6B), whereas cellular internalization of Dox showed an insignificant difference between Dox-loaded micelles and Dox/siRNA-loaded micelleplexes as determined by CLSM images and flow cytometry (Fig. S23A and S24A, B†). This difference can be attributed to the differences in cellular uptake mechanisms; specifically, free Dox only diffused into the cells passively, whereas the encapsulated Dox was delivered to the cells through caveolar endocytosis, in which the positively charged surface of the micelleplexes facilitated cellular internalization through an electrostatic interaction with the negatively charged cell membrane.[49–51] The uptake efficiency levels observed for the siRNA-condensed micelleplexes and Dox/siRNA-loaded micelleplexes were comparable as determined by CLSM images and flow cytometry (Fig. S23B and S24C, D), and they both exceeded that derived for free siRNA by fivefold (Fig. 6C). The enhanced uptake efficiency can be attributed to the fact that the protonated PDMAEMA on LB shielded the negative charge on siRNA to prevent electrostatic repulsion between the cell membrane and siRNA, in addition to being attributable to the caveolar endocytosis process facilitated by the electrostatic interaction between the positively-charged micelleplexes and negatively-charged cell membrane.

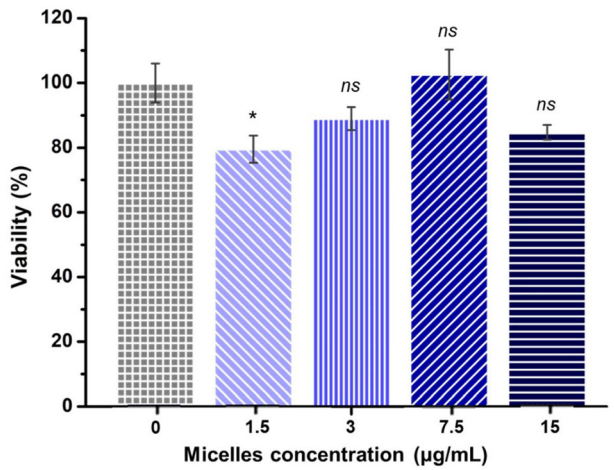

Fig. 5 Material cytotoxicity of LB micelles in MDA-MB-231 cancer cells, as evaluated using the MTT assay. MDA-MB-231 cancer cells (3000 cells per well) were treated with the LB micelles and further incubated for 24 h. Data are expressed as mean values ± SEM; *p < 0.05, ns, not significant.

In vitro downregulation of Bcl-2 mRNA

Before testing the therapeutic effects of the Dox/Bcl-2 siRNA-loaded micelleplexes, we conducted a control experiment to test the *in vitro* downregulation of Bcl-2 mRNA (an antiapoptotic gene) by Bcl-2 siRNA-loaded LB (hereafter referred to as Bcl-2 siRNA/LB) micelleplexes. To compare the effectiveness of

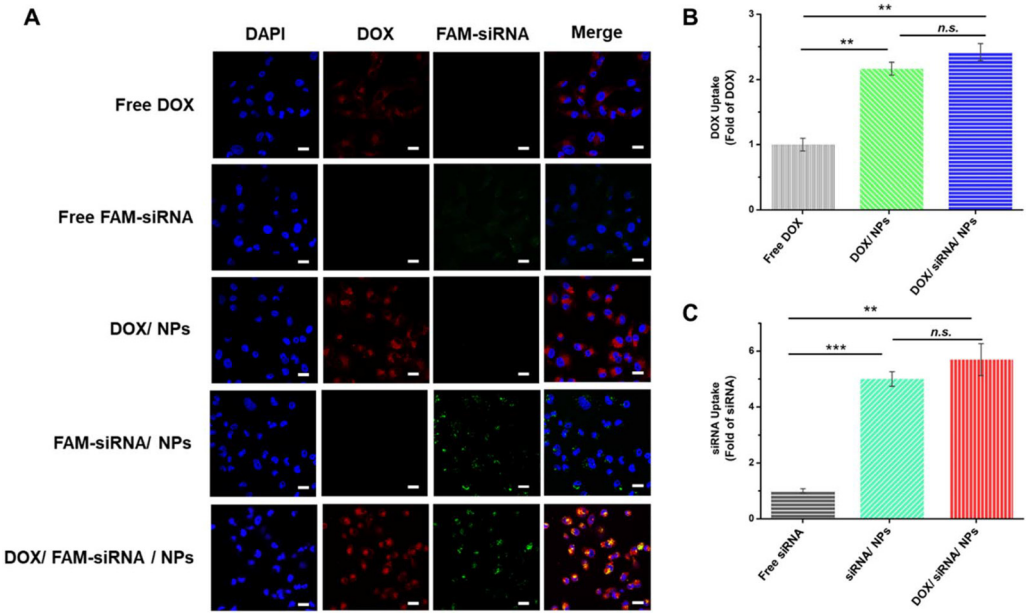

Fig. 6 Cellular uptake of FAM-labeled siRNA (75 nM) and Dox (3 μg mL^{-1}) in MDA-MB-231 cancer cells. FAM-labeled siRNA, Dox, and DAPI-labeled nuclei are visualized in green, red, and blue fluorescence, respectively. Scale bar = 20 μm. (A) Images captured using a Zeiss LSM 780 confocal microscope for MDA-MB-231 cells treated with free Dox, free FAM-labeled siRNA, Dox/LB micelles, FAM-labeled siRNA/LB micelleplexes, and Dox/FAM-labeled siRNA/LB micelleplexes. (B) Cellular uptake of Dox determined by calculating AOD in CLSM images. (C) Quantitative data of cellular uptake of FAM-labeled siRNA. Data are expressed as mean ± SEM; *$p < 0.05$, **$p < 0.01$, ***$p < 0.001$.

control siRNA-loaded LB (hereafter denoted as Ctrl siRNA/LB) micelleplexes with that of the Bcl-2 siRNA/LB micelleplexes in silencing Bcl-2 mRNA expression in MDA-MB-231 cells, we performed a quantitative real-time polymerase chain reaction (qRT-PCR) analysis. As illustrated in Fig. 7, the Bcl-2 mRNA expression in cells treated with the Ctrl siRNA/LB micelleplexes (concentration = 50 nM) was consistent with that in the control cells (*i.e.*, untreated cells). Increasing the concentration of Ctrl siRNA/LB micelleplexes to 100 nM still resulted in a nonsignificant silencing effect. However, the Bcl-2 siRNA/LB micelleplexes (concentration = 50 nM) substantially downregulated the expression of Bcl-2 mRNA, and when their concentration was increased to 100 nM, the Bcl-2 mRNA expression was further downregulated by 50%, implying that siRNA delivered by PEG-*b*-PDMAEMA-*b*-PDPA should be effective for the downregulation of Bcl-2 mRNA expression.

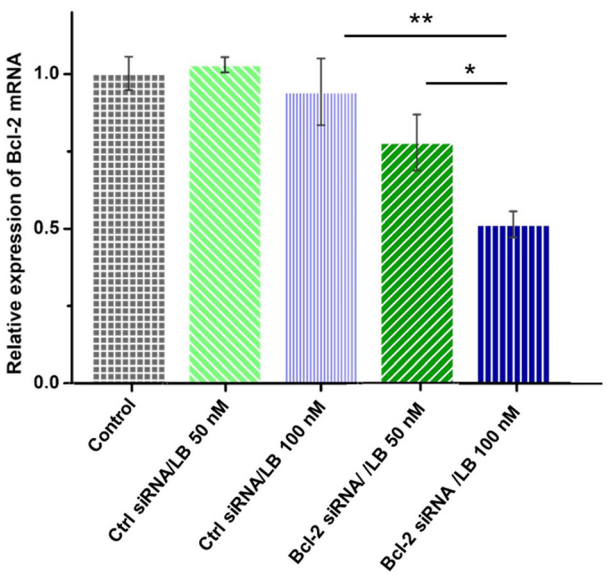

Fig. 7 Expression of Bcl-2 mRNA, as evaluated using qRT-PCR, in MDA-MB-231 treated with Ctrl siRNA/LB micelleplexes and Bcl-2 siRNA/LB micelleplexes at siRNA concentrations of 50 and 100 nM. Data are expressed as mean values ± SEM; *$p < 0.05$, **$p < 0.01$.

In vitro combination therapy of pH-responsive, two-in-One Dox/Bcl-2 siRNA-loaded micelleplexes

To demonstrate the effectiveness of PEG-*b*-PDMAEMA-*b*-PDPA copolymers in simultaneously delivering Dox and siRNA for combination therapy, we compared the therapeutic efficiency of Dox/Bcl-2 siRNA-loaded LB (hereafter denoted as Dox/Bcl-2 siRNA/LB) micelleplexes with that of Ctrl siRNA/LB micelleplexes, Bcl-2 siRNA/LB micelleplexes, and Dox/control siRNA-loaded LB (hereafter denoted as Dox/Ctrl siRNA/LB) micelleplexes. Therapeutic efficiency was evaluated using the MTT assay to determine MDA-MB-231 cell viability after treatment with the various micelleplexes (Fig. 8). At a siRNA concentration of 50 nM, the cells treated with the Ctrl siRNA/LB and Dox/Ctrl siRNA/LB micelleplexes exhibited high viability (>80%); this is because the Ctrl siRNA/LB micelleplexes could not downregulate mRNA expression and because the Dox concentration in the Dox/Ctrl siRNA/LB micelleplexes was too low (1 μg mL^{-1}) to induce substantial cytotoxicity. The Bcl-2 siRNA/LB micelleplexes could inhibit the expression of mRNA

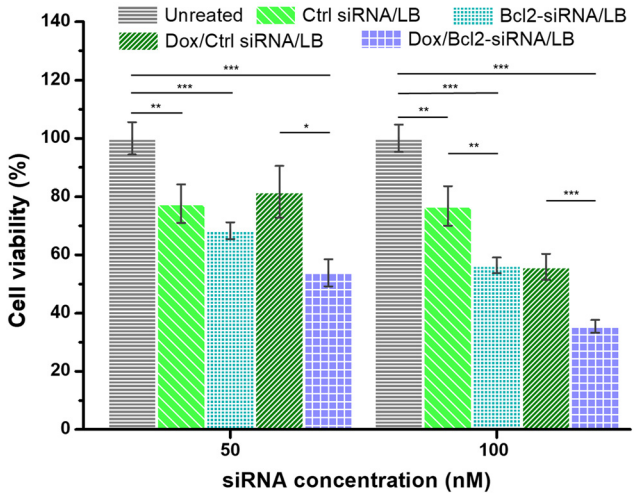

Fig. 8 Cell viability of MDA-MB-231 cancer cells treated with Ctrl-siRNA/LB, Bcl-2 siRNA/LB, Dox/Ctrl-siRNA/LB, and Dox/Bcl-2 siRNA/LB micelleplexes at siRNA concentrations of 50 and 100 nM. Data are expressed as mean values ± SEM; $*p < 0.05$, $**p < 0.01$, $***p < 0.001$.

and thus engendered a lower cell viability rate (approximately 68%). The cells treated with the Dox/Bcl-2 siRNA/LB micelleplexes had a cell viability of 54%, which can be attributed to the combined effects of Dox and siRNA in suppressing Bcl-2, a gene that sensitizes drug-resistant TNBC cells to Dox. Furthermore, Dox/Bcl-2 siRNA/LB micelleplexes effectively induced cell apoptosis determined by FITC Annexin V assay *via* flow cytometry (Fig. S25 and 26), whereas Ctrl siRNA/LB showed an insignificant effect on MDA-MB-231 cells in comparison with the control group without treatment. When the siRNA concentration was raised to 100 nM, the Bcl-2 siRNA/LB, Dox/Ctrl siRNA/LB, and Dox/Bcl-2 siRNA/LB micelleplexes (but not the Ctrl siRNA/LB micelleplexes) exhibited enhanced therapeutic efficiency, matching the expectation that the Ctrl siRNA acts as a blank. The viability of the MDA-MD-231 cells treated with the Bcl-2 siRNA/LB micelleplexes dropped from 68% to 56%; this is because 100 nM Bcl-2 siRNA could effectively activate the RISC to suppress the growth of MDA-MB-231 cancer cells through the inhibition of antiapoptotic mechanisms. The viability of the cells treated with the Dox/Ctrl siRNA/LB micelleplexes was reduced from 82% to 56%; this can be attributed to the elevated Dox concentration (from 1 to 2 μg mL^{-1}), which exceeded the drug tolerance of the cancer cells and thus led to cell apoptosis. In particular, the Dox/Bcl-2 siRNA/LB micelleplexes exhibited the highest therapeutic efficacy in that they reduced the viability of the cells to 36%, demonstrating the effectiveness of combining chemotherapy and gene therapy for TNBC treatment.

Conclusions

We synthesized a series of block and random copolymers to prepare a two-in-one pH-responsive drug delivery system that can carry both Dox and siRNA to achieve combination chemotherapy and gene therapy. Considering the importance of a well-defined block copolymer structure and an adequate cationic block chain length for Dox and siRNA loading, we selected the PEG_{113}-*b*-$PDMAEMA_{55}$-*b*-$PDPA_{59}$ (LB) block copolymer, which had the longest PDMAEMA chain and the highest Dox and Bcl-2 siRNA loading efficiency levels (DLE = 86.9% and 93%, respectively), as the carrier. We encapsulated the LB copolymer with Dox and Bcl-2 siRNA to form Dox/Bcl-2 siRNA-loaded micelleplexes, which were stable at pH 7.4 and exhibited Dox and siRNA cumulative release efficiency levels of 24% and 15% within 24 h. Changing the pH value from 7.4 to 5.0 resulted in a burst release, which increased the cumulative release efficiency of Dox and siRNA to approximately 69% and 59%, respectively, within 24 h. Control studies confirmed that PEG_{113}-*b*-$PDMAEMA_{55}$-*b*-$PDPA_{59}$ concentrations below 15 μg mL^{-1} had negligible cytotoxicity, that the Dox/Bcl-2 siRNA-loaded micelleplexes facilitated the cellular internalization of Dox and siRNA, and that Bcl-2 siRNA/LB micelleplexes were effective in suppressing antiapoptotic mechanisms through the downregulation of Bcl-2 mRNA expression. As revealed by our *in vitro* test of therapeutic efficiency, the Dox/Bcl-2 siRNA-loaded micelleplexes could effectively deliver Dox and Bcl-2 siRNA simultaneously and produced the lowest cell viability (36%) compared with the Dox/Ctrl-siRNA/LB micelleplexes (56%) and Bcl-2 siRNA/LB micelleplexes (56%). Although we used Dox as the chemotherapy drug and Bcl-2 siRNA for TNBC treatment in this study, PEG_{113}-*b*-$PDMAEMA_{55}$-*b*-$PDPA_{59}$ can encapsulate a wide variety of hydrophobic chemotherapeutics and siRNAs. Moreover, considering the pH-responsive behavior of PEG_{113}-*b*-$PDMAEMA_{55}$-*b*-$PDPA_{59}$, for which the phase transition pH was 6.88 and pH interval was 0.24, we anticipate that delivery systems based on PEG-*b*-PDMAEMA-*b*-PDPA will constitute a versatile pH-responsive platform for encapsulating both chemotherapy drugs and siRNA for combination therapy for TNBC treatment.

Conflicts of interest

The authors declare no competing financial interests.

Acknowledgements

We thank the Ministry of Science and Technology of the Republic of China (MOST 108-2628-M-007-003-MY2) for funding this research. We also thank the Ministry of Science and Technology of the Republic of China (MOST 110-2634-F-007-023) and the Frontier Research Center on Fundamental and Applied Sciences of Matters, Ministry of Education, Taiwan, for supporting this research. This work was financially supported by the "Frontier Research Center on Fundamental and Applied Sciences of Matters," part of the Featured Areas Research Center Program within the framework of the Higher Education Sprout Project by the Ministry of Education (MOE)

in Taiwan. We are also grateful to Professor Hsin-Lung Chen in the Department of Chemical Engineering at National Tsing Hua University for the assistance in dynamic light scattering (DLS) measurement. Malvern Instrument (Nano S) is supported by the Department of Chemical Engineering at National Tsing Hua University. We thank Professor Kui-Thong Tan in the Department of Chemistry at National Tsing Hua University for assistance in agarose gel electrophoresis.

References

1 N. Vasan, J. Baselga and D. M. Hyman, *Nature*, 2019, **575**, 299–309.
2 J. Shi, P. W. Kantoff, R. Wooster and O. C. Farokhzad, *Nat. Rev. Cancer*, 2017, **17**, 20–37.
3 D. Hanahan and R. A. Weinberg, *Cell*, 2011, **144**, 646–674.
4 R. Dent, M. Trudeau, K. I. Pritchard, W. M. Hanna, H. K. Kahn, C. A. Sawka, L. A. Lickley, E. Rawlinson, P. Sun and S. A. Narod, *Clin. Cancer Res.*, 2007, **13**, 4429–4434.
5 T. C. de Ruijter, J. Veeck, J. P. J. de Hoon, M. van Engeland and V. C. Tjan-Heijnen, *J. Cancer Res. Clin. Oncol.*, 2011, **137**, 183–192.
6 L. Carey, E. Winer, G. Viale, D. Cameron and L. Gianni, *Nat. Rev. Clin. Oncol.*, 2010, **7**, 683–692.
7 W. D. Foulkes, I. E. Smith and J. S. Reis-Filho, *N. Engl. J. Med.*, 2010, **363**, 1938–1948.
8 S. A. O'Toole, J. M. Beith, E. K. A. Millar, R. West, A. McLean, A. Cazet, A. Swarbrick and S. R. Oakes, *J. Clin. Pathol.*, 2013, **66**, 530.
9 W. J. Irvin and L. A. Carey, *Eur. J. Cancer*, 2008, **44**, 2799–2805.
10 E. H. Jeong, H. Kim, B. Jang, H. Cho, J. Ryu, B. Kim, Y. Park, J. Kim, J. B. Lee and H. Lee, *Adv. Drug Delivery Rev.*, 2016, **104**, 29–43.
11 R. Kanasty, J. R. Dorkin, A. Vegas and D. Anderson, *Nat. Mater.*, 2013, **12**, 967–977.
12 A. Wittrup and J. Lieberman, *Nat. Rev. Genet.*, 2015, **16**, 543–552.
13 S.-Y. Qin, Y.-J. Cheng, Q. Lei, A.-Q. Zhang and X.-Z. Zhang, *Biomaterials*, 2018, **171**, 178–197.
14 Q. Hu, W. Sun, C. Wang and Z. Gu, *Adv. Drug Delivery Rev.*, 2016, **98**, 19–34.
15 B. Al-Lazikani, U. Banerji and P. Workman, *Nat. Biotechnol.*, 2012, **30**, 679–692.
16 M. Saraswathy and S. Gong, *Mater. Today*, 2014, **17**, 298–306.
17 M. Creixell and N. A. Peppas, *Nano Today*, 2012, **7**, 367–379.
18 Y. Li, T. Thambi and D. S. Lee, *Adv. Healthcare Mater.*, 2018, **7**, 1700886.
19 Y. J. Kwon, *Acc. Chem. Res.*, 2012, **45**, 1077–1088.
20 J. Nguyen and F. C. Szoka, *Acc. Chem. Res.*, 2012, **45**, 1153–1162.
21 M. A. Behlke, *Mol. Ther.*, 2006, **13**, 644–670.
22 C. V. Pecot, G. A. Calin, R. L. Coleman, G. Lopez-Berestein and A. K. Sood, *Nat. Rev. Cancer*, 2011, **11**, 59–67.
23 E. Wagner, *Acc. Chem. Res.*, 2012, **45**, 1005–1013.
24 G. Navarro, J. Pan and V. P. Torchilin, *Mol. Pharm.*, 2015, **12**, 301–313.
25 M. K. Grun, A. Suberi, K. Shin, T. Lee, V. Gomerdinger, Z. M. Moscato, A. S. Piotrowski-Daspit and W. M. Saltzman, *Biomaterials*, 2021, **272**, 120780.
26 R. Kumar, C. F. S. Chalarca, M. R. Bockman, C. V. Bruggen, C. J. Grimme, R. J. Dalal, M. G. Hanson, J. K. Hexum and T. M. Reineke, *Chem. Rev.*, 2021, **121**, 11527–11652.
27 D. Sprouse, Y. Jiang, J. E. Laaser, T. P. Lodge and T. M. Reineke, *Biomacromolecules*, 2016, **17**, 2849–2859.
28 Z. Tan, Y. Jiang, W. Zhang, L. Karls, T. P. Lodge and T. M. Reineke, *J. Am. Chem. Soc.*, 2019, **141**, 15804–15817.
29 A. Sizovs, L. Xue, Z. P. Tolstyka, N. P. Ingle, Y. Wu, M. Cortez and T. M. Reineke, *J. Am. Chem. Soc.*, 2013, **135**, 15417–15424.
30 H. Li, M. A. Cortez, H. R. Phillips, Y. Wu and T. M. Reineke, *ACS Macro Lett.*, 2013, **2**, 230–235.
31 Y. Jiang, T. P. Lodge and T. M. Reineke, *J. Am. Chem. Soc.*, 2018, **140**, 11101–11111.
32 D. Sprouse and T. M. Reineke, *Biomacromolecules*, 2014, **15**, 2616–2628.
33 Y. Wu, M. Wang, D. Sprouse, A. E. Smith and T. M. Reineke, *Biomacromolecules*, 2014, **15**, 1716–1726.
34 Y. Jiang, D. Sprouse, J. E. Laaser, Y. Dhande, T. M. Reineke and T. P. Lodge, *J. Phys. Chem. B*, 2017, **121**, 6708–6720.
35 Y. Jiang, T. M. Reineke and T. P. Lodge, *Macromolecules*, 2018, **51**, 1150–1160.
36 R. J. Dalal, R. Kumar, M. Ohnsorg, M. Brown and T. M. Reineke, *ACS Macro Lett.*, 2021, **10**, 886–893.
37 J. E. Laaser, E. Lohmann, Y. Jiang, T. M. Reineke and T. P. Lodge, *Macromolecules*, 2016, **49**, 6644–6654.
38 C. E. Nelson, J. R. Kintzing, A. Hanna, J. M. Shannon, M. K. Gupta and C. L. Duvall, *ACS Nano*, 2013, **7**, 8870–8880.
39 T. A. Werfel, M. A. Jackson, T. E. Kavanaugh, K. C. Kirkbride, M. Miteva, T. D. Giorgio and C. Duvall, *J. Controlled Release*, 2017, **255**, 12–26.
40 K. Matyjaszewski and J. Xia, *Chem. Rev.*, 2001, **101**, 2921–2990.
41 K. Landfester, *Angew. Chem., Int. Ed.*, 2009, **48**, 4488–4507.
42 H.-H. Lu, C.-H. Huang, T.-Y. Shiue, F.-S. Wang, K.-K. Chang, Y. Chen and C.-H. Peng, *Chem. Sci.*, 2018, **10**, 284–292.
43 K. Zhou, Y. Wang, X. Huang, K. Luby-Phelps, B. D. Sumer and J. Gao, *Angew. Chem., Int. Ed.*, 2011, **50**, 6109–6114.
44 K. Zhou, H. Liu, S. Zhang, X. Huang, Y. Wang, G. Huang, B. D. Sumer and J. Gao, *J. Am. Chem. Soc.*, 2012, **134**, 7803–7811.
45 Q. Feng, J. Wilhelm and J. Gao, *Acc. Chem. Res.*, 2019, **52**, 1485–1495.
46 C. Kong, Y. Li, Z. Liu, J. Ye, Z. Wang, L. Zhang, W. Kong, H. Liu, C. Liu, H. Pang, Z. Hu, J. Gao and F. Qian, *ACS Nano*, 2019, **13**, 4049–4063.
47 Y. Li, T. Zhao, C. Wang, Z. Lin, G. Huang, B. D. Sumer and J. Gao, *Nat. Commun.*, 2016, **7**, 13214.

48 L. Han, C. Tang and C. Yin, *Biomaterials*, 2015, **60**, 42–52.
49 S. Han, Q. Cheng, Y. Wu, J. Zhou, X. Long, T. Wei, Y. Huang, S. Zheng, J. Zhang, L. Deng, X. Wang, X.-J. Liang, H. Cao, Z. Liang and A. Dong, *Biomaterials*, 2015, **48**, 45–55.
50 C. Wang, L. Du, J. Zhou, L. Meng, Q. Cheng, C. Wang, X. Wang, D. Zhao, Y. Huang, S. Zheng, H. Cao, J. Zhang, L. Deng, Z. Liang and A. Dong, *ACS Appl. Mater. Interfaces*, 2017, **9**, 32463–32474.
51 D. J. Gary, H. Lee, R. Sharma, J.-S. Lee, Y. Kim, Z. Y. Cui, D. Jia, V. D. Bowman, P. R. Chipman, L. Wan, Y. Zou, G. Mao, K. Park, B.-S. Herbert, S. F. Konieczny and Y.-Y. Won, *ACS Nano*, 2011, **5**, 3493–3505.